Pharm Res (2011) 28:1167–1178
DOI 10.1007/s11095-011-0381-1

RESEARCH PAPER

Octreotide-Modified Polymeric Micelles as Potential Carriers for Targeted Docetaxel Delivery to Somatostatin Receptor Overexpressing Tumor Cells

Yuan Zhang • Xueqing Wang • Jiancheng Wang • Xuan Zhang • Qiang Zhang

Received: 8 August 2010 / Accepted: 24 January 2011 / Published online: 22 February 2011

ABSTRACT

Purpose Somatostatin analogue octreotide (OCT)-modified PEG-*b*-PLA micelles were constructed to bind to somatostatin receptors (SSTRs) overexpressed on tumor cells for enhanced intracellular drug delivery and improved therapeutic efficacy for malignant tumors.

Methods Copolymers conjugated with octreotide (OCT-PEG_{6000}-*b*-PLA_{5000}) were synthesized. The fluorescent probe DiI or docetaxel (DTX)-loaded micelles with or without octreotide modification (OCT-PM-DiI, PM-DiI, OCT-PM-DTX and PM-DTX) were prepared, and their physiochemical properties, intracellular delivery *in vitro* or anti-tumor activity *in vivo* were evaluated, respectively.

Results The CMC of OCT-PEG_{6000}-*b*-PLA_{5000} was quite low ($<10^{-6}$ mol/L). All micelles were less than 80 nm with spherical shape and high encapsulation efficiency. DTX molecules were well dispersed in the micelles without chemical interactions with the polymers. Flow cytometry and confocal microscopy results showed that OCT-PM-DiI enhanced intracellular delivery efficiency via receptor-mediated endocytosis in NCI-H446 cells; the optimal modification ratio of OCT on micelle surface was 5%. OCT-PM-DTX exhibited higher retardation of tumor growth after intravenous injections into xenograft NCI-H446 tumor model; octreotide-modified micelles did not show severe toxicity.

Conclusions SSTRs targeting micelles may serve as promising nanocarriers in tumor treatment for hydrophobic anticancer drugs, such as DTX.

KEY WORDS antitumor efficacy · DTX · intracellular delivery · octreotide · polymeric micelles

Y. Zhang (✉) · X. Wang · J. Wang · X. Zhang · Q. Zhang (✉)
State Key Laboratory of Natural and Biomimetic Drugs
School of Pharmaceutical Sciences, Peking University
38 Xueyuan Road, Haidian District
Beijing 100191, People's Republic of China
e-mail: sinoyuan11@gmail.com

Q. Zhang
e-mail: zqdodo@bjmu.edu.cn

INTRODUCTION

The clinical application of some traditional chemotherapeutic agents is limited due to their poor water solubility and intolerable side effects on patients. Docetaxel (DTX) is an anticancer drug that is widely used due to its excellent therapeutic effects against a wide spectrum of cancers. It is a semi-synthetic taxane analog superior to paclitaxel. Docetaxel has a greater affinity to β-tubulin binding site, wider cell-cycle bioactivity and an increased uptake with slower efflux from the tumor cells, thus resulting in longer intracellular retention time and higher intracellular concentrations. The solubility of DTX is extremely low, so Tween-80 and ethanol are included in Taxotere® to solubilize DTX (1). Such formulation is also non-specific in drug distribution, and it is found to cause many side effects after intravenous injection or infusion in clinical application due to DTX itself as well as Polysorbate 80, including pruritus, systemic anaphylaxis, low blood-cell counts, bruising or bleeding, anemia, nausea, vomiting, sore mouth or mouth ulcers, taste changes, diarrhea, hair loss, skin changes, hand-foot syndrome, tiredness and fluid retention (edema) (2,3).

Thus, it is highly desirable to develop new drug delivery systems that can enhance the efficacy of chemotherapeutic agents, while limiting their side effects on normal tissues. During the last several years, significant developments have

been made with targeted drug delivery (4–6), which led to the accumulation of anticancer agents in high concentrations specifically at the tumor site, limiting their distribution to other tissues and organs.

Polymeric micelles are formed by block copolymers typically consisting of hydrophilic and hydrophobic chains (7). Micelles are widely used as nanocarriers because of their efficacy in encapsulating a large amount of hydrophobic drugs within the inner core, their stability in the blood circulation and their ability to gradually release the loaded drugs (8). The small particle sizes of polymeric micelles (10–100 nm) allow them to evade uptake by the reticuloendothelial system (RES) (9) and facilitate drug delivery at the tumor site by enhanced permeability and retention (EPR) effects (10). In our study, PEG-*b*-PLA micelles were used as delivery carriers of the hydrophobic anticancer drug. As the hydrophobic part of the amphiphilic polymer, PLA, approved by the Food and Drug Administration (FDA), has been well-studied due to its good biodegradation and biocompatibility, while the polyethylene glycol (PEG), being the hydrophilic section, is non-toxic and non-immunogenic. PEG improves the physicochemical and biological properties of micelles, resulting in longer circulation time *in vivo*. PEG creates a hydrophilic protective layer around the nanoparticles, which is able to repel the absorption of opsonin proteins via steric repulsion forces, thereby blocking or delaying the first step in the opsonization process. PEG also reduces aggregation of the micelle particles and inhibits their interactions with serum proteins (11,12).The solubility of DTX would be greatly increased by more than 1000-fold after its encapsulation in the micelle vectors, which renders a high concentration in aqueous solution without the addition of any solubilizing agents. Previous studies indicated that DTX-loaded micelles showed stronger cytotoxicity to different tumor cell lines *in vitro* and greater tumor suppression effect with less toxicity *in vivo* than conventional formulations (3).

Somatostatin (SST) is a regulatory peptide endogenously produced in neuroendocrine and immune cells. It regulates a variety of physiological functions, including potent inhibition of hormone and growth factor secretion, which promote tumor growth, as well as modulation of cell proliferation, leading to growth arrest and induction of apoptosis (13). These biological effects are thought to be mediated by five somatostatin receptor subtypes (SSTR1-5). SSTRs are members of the G-protein-coupled receptors (GPCR) superfamily, which are widely distributed in a variety of tumors and cancer cell lines, including small-cell lung cancer (14,15), neuroendocrine tumors (16,17), prostate cancer, breast cancer (18), colorectal carcinoma, gastric cancer and hepatocellular carcinoma (19). SST and its analogs bind to the SSTRs specifically with high affinity in the low nanomolar range to produce a broad spectrum of biological effects in many mammary cancer models.

The radiolabeled peptides are used *in vivo* receptor scintigraphy to label the location of tumors and their metastases, and it also emerges as a serious treatment option at the therapeutic level. Many somatostatin analogs labeled with radionuclide (eg. ^{111}In-, ^{90}Y-, ^{177}Lu-, ^{68}Ga-) have shown a reduction or at least a stabilization of tumor growth after intravenous injection (20).The peptides conjugated to cytotoxic agents have also been attempted for antitumor therapy (21).

Octreotide (OCT) is one of the most extensively studied SST analogs, selectively binding to SSTR2, SSTR5, especially more to SSTR2, and less to SSTR3 (22). Many studies have demonstrated that OCT is practically valuable in developing the tumor tracers and the delivery systems for anticancer drugs (23). The half life of octreotide in plasma is much longer than endogenous SST (eg.SST-14 and SST-28) (22), ensuring longer biological effect *in vivo* and preventing immediate clearance in blood circulation. In light of the above facts, OCT was introduced here as the targeting bullet conjugated on the surface of micellar nanoparticles to achieve enhanced intracellular delivery of chemotherapeutic agent and superior antitumor efficacy towards specific malignant tumor model.

In this study, we designed and prepared octreotide-modified and DTX-loaded PEG-*b*-PLA polymeric micelles (OCT-PM-DTX) for the first time in order to achieve SSTRs-mediated cell-/tissue-specific targeting delivery for cancer therapy. The fluorescent probe DiI-loaded micelles with OCT modification (OCT-PM-DiI) were prepared and tested on SSTRs overexpressing small-cell lung cancer cell line (NCI-H446) to detect the intracellular internalization, targeting delivery efficiency and cellular uptake mechanism. Tumor selectivity and antitumor efficacy of OCT-PM-DTX were evaluated on xenograft BALB/c nude mice bearing NCI-H446 cells after intravenous injection.

MATERIALS AND METHODS

Materials

PEG_{5000}-*b*-PLA_{5000} (Mw/Mn = 1.11 as determined by GPC) and N-hydroxy-succinimidy-PEG_{6000}-*b*-PLA_{5000} (NHS-PEG_{6000}-*b*-PLA_{5000}, Mw/Mn = 1.35 determined by GPC) were purchased from Advanced Polymer Materials Inc. (Montreal, QC, Canada). OCT was from Zaichuang Biotechnical Inc. (Shanghai, China), and DTX was from Kejiegaoxin Technical Inc. (Chengdu, Sichuan, China). Ninhydrin (Fluka) was from Sigma; dialysis bag (molecular weight cut off = 3500 Da) was from JingKeHongDa Biotechnology Co., Ltd (China). Triethylamine (TEA), trifluoroacetic acid (TFA), uranyl acetate, acetonitrile were

all commodity chemicals of analytical grade. 1,1'-dioctadecyl-3,3,3',-3'-tetramethylindocarbocyanine perchlorate (DiI) and Hoechst33258 were supplied by Molecular Probes Incorporation (Eugene, Oregon, USA). Goat antihuman SSTR2 polyclonal antibody was purchased from Santa Cruz Biotechnology Inc. (CA, USA). Tween 80 was from Sigma Corporation (USA). Penicillin-streptomycin was supplied by GIBCO, Invitrogen Corporation (Carlsbad, California, USA). Fetal bovine serum (FBS) was purchased from Sijiqing Company (Hangzhou, China). Trypsin was from Biodee Biotechnology Co., Ltd. (Beijing, China). Sterile filters (0.2 μm) were purchased from Sartorius Stedim Biotech Company (Germany). All other reagents were of analytical grade.

Synthesis and Characterization of Octreotide-Modified Block Copolymer

The NHS-PEG$_{6000}$-*b*-PLA$_{5000}$ was used to conjugate OCT to the distal end of PEG hydrophilic segment of the block copolymers. This reaction takes place via nucleophilic chemical reaction by replacing NHS group with the primary amino group of octreotide to form a stable amido bond (Fig. 1). OCT and NHS-PEG$_{6000}$-*b*-PLA$_{5000}$ (1/2, mol/mol) were dissolved in DMSO (1 mg/mL for octreotide) (24). TEA (TEA/NHS-PEG$_{6000}$-*b*-PLA$_{5000}$ = 3/1, mol/mol) was added to adjust the pH value of DMSO reaction solvent to 8–9. The reaction proceeded for 1 h at room temperature under moderate stirring. Thin layer chromatography (TLC) was applied to trace the reaction process qualitatively by ninhydrin method (25). The developing solvent was 1-butanol/33% acetic acid = 1/1 (*v*/*v*). When the reaction completed, the reaction mixture was dialyzed in a dialysis bag extensively against distilled water for 24 h to remove the unconjugated OCT, DMSO and other impurities. The final solution was lyophilized and stored at −20°C before use.

Reverse-phase HPLC was applied to quantify the conjugation efficiency of OCT. At appropriate reaction time points, 20 μL reacting mixture was drawn from the reaction solvent and diluted to 200 μL by the mobile phase. Then, the OCT in sample solution was assayed by an HPLC system (reverse-phase C18 column, 4.6 mm × 250 mm, 5 μm; Shimadzu, LC-10AT, Japan) at a flow rate of 1.0 mL/min, and detected at 220 nm. The mobile phase was a mixture of acetonitrile/pH 7.4 PBS (30/70, *v*/*v*) containing 0.1% TFA. The OCT conjugation efficiency was calculated by the following formula:

$$\textit{Conjugation Efficiency}\ (\%) = \frac{A - B}{A} \times 100$$

A represents the amount of OCT at the initial reaction time, and *B* is the amount of OCT at the end of reaction.

The formation and the molecular weight distribution of synthesized OCT-PEG$_{6000}$-*b*- PLA$_{5000}$ were determined by gel permeation chromatography (GPC), calibrated with PEG standards, with THF as eluent at a flow rate of 1.0 mL/min. The CMC of PEG$_{5000}$-*b*-PLA$_{5000}$ and OCT-PEG$_{6000}$-*b*-PLA$_{5000}$ were evaluated by a pyrene fluorescence probe technique (26).

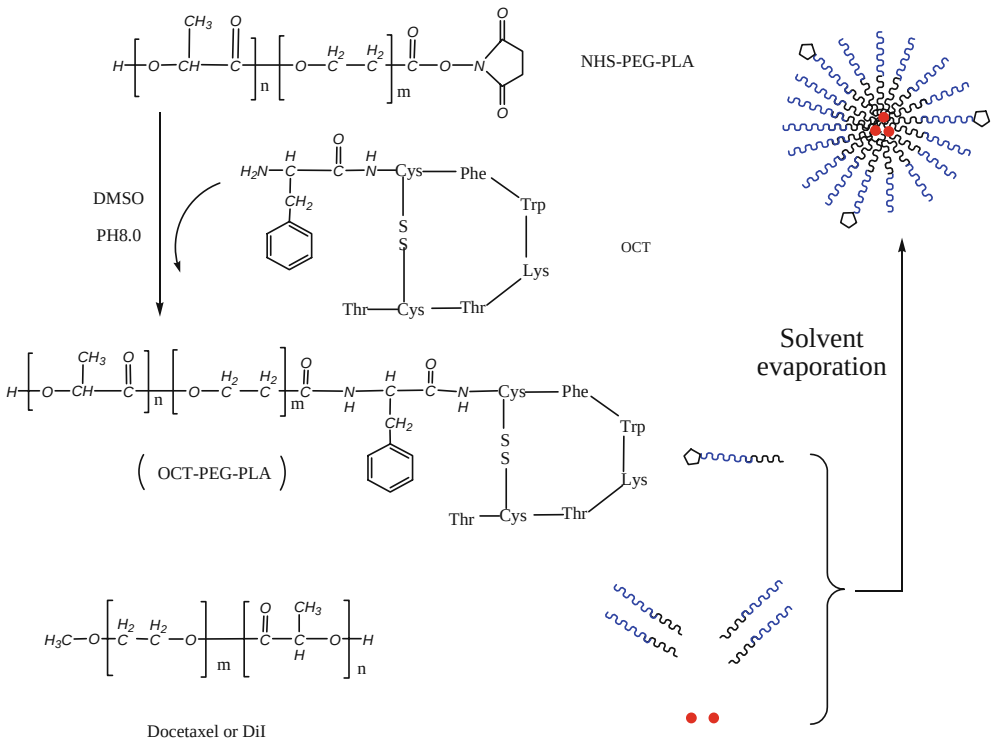

Fig. 1 Schematic representation of synthesis of OCT-PEG-*b*-PLA copolymer and the strategy of encapsulating DTX or DiI.

Preparation and Characterization of the DTX-Loaded Micelles

To prepare the OCT-PM-DTX, DTX, OCT-PEG_{6000}-*b*-PLA_{5000} and PEG_{5000}-*b*-PLA_{5000} (1/2/18, w/w/w) were dissolved in acetonitrile, and acetonitrile was evaporated under reduced pressure with a rotary evaporator at 60°C, forming a thin film in a round-bottom flask. The dried copolymer film was hydrated in 60°C distilled water and sonicated in a bath-type sonicator until a clear micelle solution was obtained. The final concentration of the total OCT-PEG_{6000}-*b*-PLA_{5000} and PEG_{5000}-*b*-PLA_{5000} is 10 mg/mL. Then, the micelle solution was centrifuged at 10,000 rpm for 5 min to precipitate the unloaded DTX, and the supernatant was extruded through a polycarbonate filter (0.22 μm pore size). The micelles obtained were stored at 4°C before use. For the preparation of PM-DTX, an identical procedure was performed except that the equivalent amount of OCT-PEG_{6000}-*b*-PLA_{5000} was replaced by PEG_{5000}-*b*-PLA_{5000}.

The mean particle size, size distribution and zeta potential of the two kinds of micelles were recorded by DLS using Malvern Zetasizer Nano ZS (Malvern, UK). The DTX loading amount and encapsulation efficiency of these micelles were determined by an HPLC system (reverse-phase C18 column, 4.6 mm×250 mm, 5 μm; Shimadzu, LC-10AT, Japan). Micelle solution was dissolved in mobile phase, eluted at a flow rate of 1.0 mL/min, and detected at 230 nm. The mobile phase was a mixture of acetonitrile/water (60/40, *v/v*). TEM micrographs of the PM-DTX and OCT-PM-DTX were taken. Briefly, copper grids were coated with a drop of micelle solution with total copolymer concentration of 2 mg/ml for 2 min. After the removal of excess solution with filter paper, a drop of uranyl acetate (2% *w/v*) was added on the copper grids to provide negative staining for 1 min. Excess fluid was removed with filter paper, and copper grids dried. The samples were finally observed under a transmission electron microscope (JEM-100CX, Japan) at a magnification of 61,000 (27).

XRD measurements of DTX powder, lyophilized blank micelles and lyophilized DTX-loaded micelles were carried out on a Rigaku Dmax/2400 X-ray diffractometer with CuKα radiation (λ=1.5406 Å) at room temperature (28). The scanning speed was 4°C/min, and the XRD patterns were recorded by scanning 2θ angles from 3° to 50° in scan mode (0.02°) at 40 kV and 100 mA. The slit widths were set at 1/2° for DS, 1/2° for SS and 0.3 mm for RS.

FTIR spectra were recorded on NEXUS-470 Fourier Transform Infrared Spectrometer (Thermo Nicolet Corporation) over the range of 400–4000 cm^{-1} by accumulating 32 scans at a resolution of 8 cm^{-1} with sample gain of 8.0, mirror velocity of 0.6329 and aperture of 100.00. In each experiment, DTX powder, lyophilized blank micelles and lyophilized DTX-loaded micelles were mixed with potassium bromide at a ratio of 1/99 (w/w) to make into discs before measurements.

Preparation and Characterization of OCT-PM-DiI and PM-DiI

DiI was dissolved in anhydrous ethyl alcohol to obtain the stock solution (1 mg/mL). DiI and PEG-*b*-PLA (1/1,000, *w/w*) were dissolved in acetonitrile (29), and the OCT-PM-DiI (OCT-PEG_{6000}-*b*-PLA_{5000}/PEG_{5000}-*b*-PLA_{5000}=1/9, *w/w*) and PM-DiI were prepared with the same method as OCT-PM-DTX and PM-DTX mentioned above. The particle size, size distribution and zeta potential of DiI-loaded micelles were determined by DLS as described above. An aliquot of DiI-loaded micelle solution was diluted by DMSO before quantifying the DiI encapsulation efficiency via fluorescence spectroscopy with excitation wavelength set at 550 nm and emission wavelength set at 565 nm.

Cell Culture

NCI-H446 small-cell lung cancer cells were obtained from Institute of Basic Medical Sciences Chinese Academy of Medical Sciences & School of Basic Medicine Peking Union Medical College (Beijing, China). NCI-H446 cells were maintained in RPMI-1640 culture medium. The fetal bovine serum (FBS) was added into the medium to a final concentration of 10%, and then it was supplemented by 100 U/mL penicillin and 100 μg/mL streptomycin. Cells were incubated at 37°C with the presence of 5% CO_2. Cell culture medium was replaced by fresh RPMI-1640 medium every 2–3 days. Before *in vitro* assays, the cells were rinsed by 0.25% fresh trypsin with 0.53 mM EDTA for trypsinization. The resultant cell suspensions were centrifuged for 5 min at 1,000 g, and then re-suspended in RPMI-1640 culture medium before seeding on well plates for *in vitro* cell experiments. Cells were in the logarithmic phase of growth at the time of experiments.

Flow Cytometry Studies

NCI-H446 cells were seeded in six-well plates, and incubated in the complete culture medium for 24 h before treatment. The DiI-loaded micelles were diluted by serum-free culture medium (the final polymer concentration was 1 mg/mL and the DiI concentration was 1 μg/mL) and added to each well plate after extruding through a 0.2 μm steriling pore size polycarbonate filter. Untreated cells were used as negative control. After incubating at 37°C for 1 h, 3 h and 6 h with each micelle solution, the NCI-H446 cells were washed twice with cold PBS, suspended with

trypsin, and then fixed by 4% paraformaldehyde in PBS before examination by the flow cytometer (BD FACSCanTM, BD Biosciences, USA). The fluorescence intensity of DiI delivered into the cells by the micellar vectors was excited at 530 nm and detected at 570 nm. Files were collected of 10,000 gated events and analyzed with FCS Express V3 software. Before the experiment mentioned above, the intracellular delivery efficiencies of targeted PEG-*b*-PLA micelles modified by 0%, 5%, 10% or 20% molar ratio of OCT were detected with the same procedures to determine a better OCT modifying density on the micelle surface.

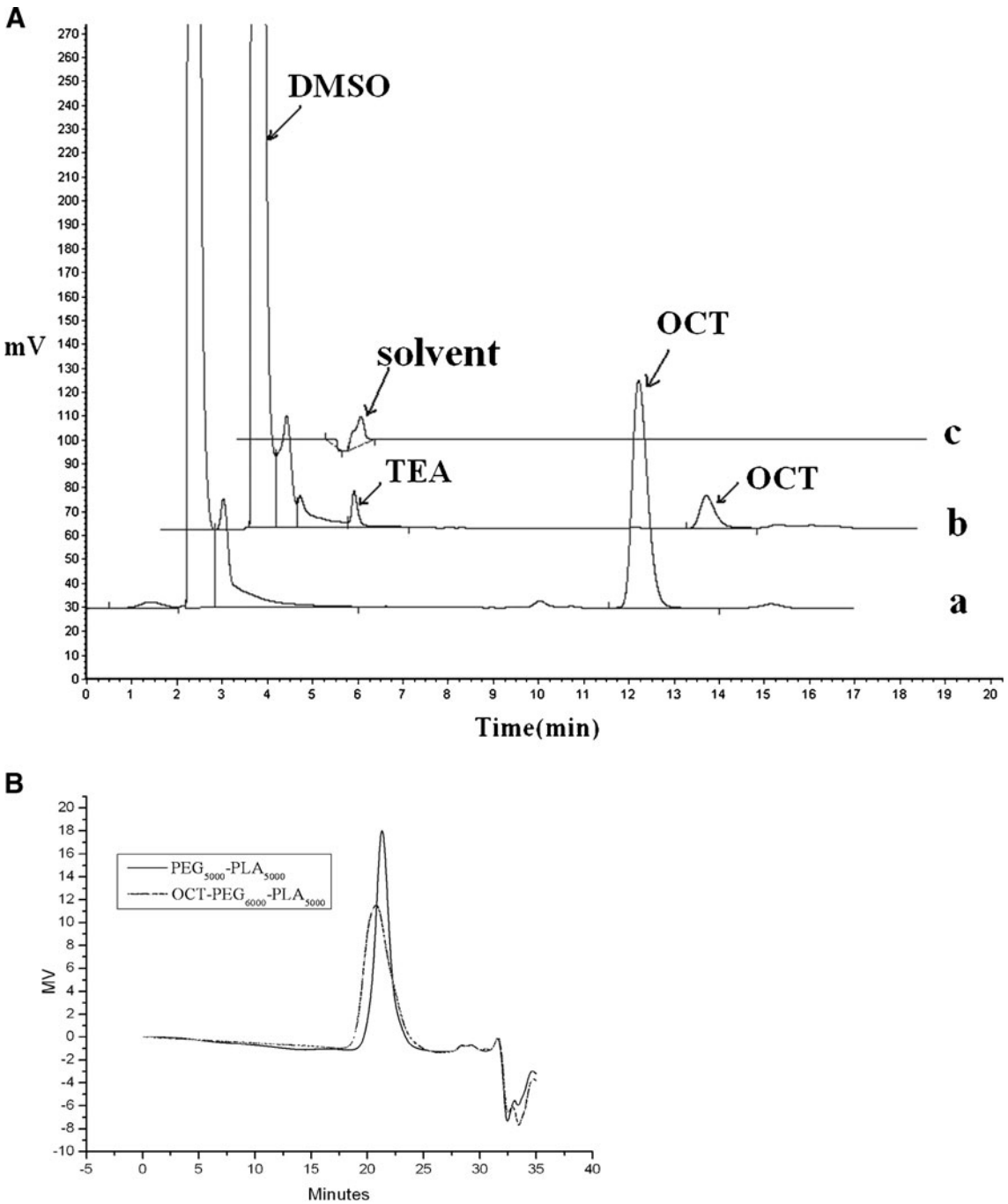

Fig. 2 Determination of OCT-PEG-*b*-PLA. (**A**) RP-HPLC assessment of unconjugated octreotide: (*a*) free OCT in reaction mixture at the initial reaction time, (*b*) NHS-PEG-*b*-PLA reacted with OCT in a molar ratio of 2:1 in the reaction mixture after reacting for 1 h at room temperature, and (*c*) lyophilized OCT-PEG-*b*-PLA product after reaction. (**B**) GPC diagram of PEG_{5000}-*b*-PLA_{5000} and the synthesized OCT-PEG_{6000}-*b*-PLA_{5000} product.

Table I Characteristics of PEG-*b*-PLA Polymeric Micelles ($n = 3$)

Polymeric micelles	Size (nm)	PDI	Zeta potential (mV)	Loading amount (%)	Encapsulation efficiency (%)
Blank PM	51.8 ± 0.7	0.04 ± 0.01	0.75 ± 0.01	–	–
PM-DTX	69.0 ± 1.0	0.2 ± 0.01	−0.13 ± 0.22	4.7 ± 0.18	98.0 ± 3.7
OCT-PM-DTX	76.4 ± 1.5	0.2 ± 0.02	−0.27 ± 0.27	3.6 ± 0.23	87.6 ± 4.8
PM-DiI	50.9 ± 0.6	0.06 ± 0.01	−1.2 ± 0.60	–	93.5 ± 4.0
OCT-PM-DiI	61.5 ± 3.1	0.07 ± 0.02	−2.8 ± 0.62	–	87.5 ± 2.1

Confocal Laser Scanning Microscope Studies

CLSM was utilized to visualize the cellular internalization and investigate the intracellular distribution of DiI-labeled micelles. NCI-H446 cells were grown on well plates to 50% confluence before treatment. The micelles were diluted by serum-free culture medium (the final polymer concentration was 1 mg/mL and the DiI concentration was 1 μg/mL) and added to each well plate after extruding through a sterile polycarbonate filter (0.2 μm pore size). After incubating at 37°C for 3 h with OCT-targeted and non-targeted micelles (30), the cells were washed three times with cold PBS, and then fixed by 4% paraformaldehyde in PBS for 10 min before the cell nucleus were stained by 2 μg/mL Hoechst 33258 (excitation/emission: 352 nm/461 nm) for 15 min. The fluorescence images, internalization of micelle-incorporated DiI as well as the fluorescence intensity of DiI delivered into the cells were visualized on a Leica TCS SP2 Confocal Laser Scanning Microscope (Germany). The excitation and emission wavelengths of fluorescent probe DiI were set at 543 nm and 565 nm, respectively. In the receptor competitive inhibition experiment, excess goat anti-human SSTR2 polyclonal antibody (1:150, primary antibody) was added to the serum-free culture medium to incubate for 1 h at 37°C prior to the addition of OCT-PM-DiI.

Pharmacodynamic Studies

The antitumor efficacies of different DTX formulations were investigated on male BALB/c nude mice (6 weeks of age, initially weighing 20–25 g) which were purchased from Vital Laboratory Animal Center (Beijing, China). All of the animal experiments adhered to the principles of Care and Use of Laboratory Animals and were approved by the Institutional Animal Care and Use Committee of Peking University. Briefly, NCI-H446 cells were collected after trypsinization and centrifugation, and then re-suspended in serum-free RPMI-1640 culture medium. Approximately 5×10^6 NCI-H446 cells were injected subcutaneously (s.c.) into the right flank of nude mice. When tumors reached 100 to 150 mm^3 in volume, mice were randomly assigned to four treatment groups ($n = 5$). The treatment formulations included OCT-PM-DTX (2.5 mg/kg), PM-DTX (2.5 mg/kg), DTX injection (2.5 mg/kg, preparation procedures referred to the formulation of Taxotere® (36)) and 5% glucose injection, which was used as negative control. Mice were administered formulations via the tail vein every two days for five times. Throughout the pharmacodynamic study, tumor volume and body weight of each mouse were monitored every two days. The tumor volumes were measured with a caliper, and calculated by the following formula: V = (major axis) × (minor

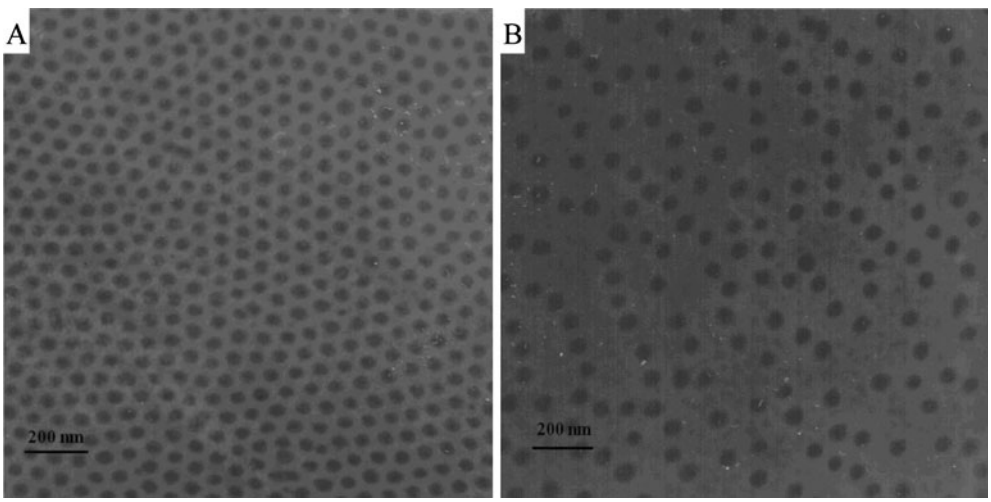

Fig. 3 TEM micrograph of PM-DTX (**A**) and OCT-PM-DTX (**B**).

axis)$^2 \times 1/2$. After the final administration, the mice were further observed for another week before they were sacrificed on the fourteenth day, and the tumors were stripped from the mice bodies. Photos of the stripped tumors of each treatment group were taken.

Statistics

Data were presented as the mean ± standard deviation (SD). Student's *t*-test and one-way analysis of variance (ANOVA) were performed in statistical evaluation to determine significance between groups. A value of $p<0.05$ was considered to be significant.

RESULTS

Synthesis and Characterization of OCT-Modified Block Copolymer

After 1 h reaction at room temperature, the dot of free OCT in the reaction mixture almost disappeared on the TLC plate, compared to that at the initial time (data not shown). The HPLC measurement showed that the conjugation efficiency of OCT was more than 85% after 1 h reaction (Fig. 2A), and the final OCT conjugation efficiency reached to 95.3% after constantly reacting for 8 h at room temperature. Thus, the molar ratio of OCT-PEG_{6000}-*b*-PLA_{5000} in the final reaction product was approximately 50%.

The molecular weights of the copolymers determined by GPC a shown in Fig. 2B. The peak value (molecular weight) of OCT-PEG_{6000}-*b*-PLA_{5000} was larger than that of PEG_{5000}-*b*-PLA_{5000}, and the retention time of OCT-PEG_{6000}-*b*-PLA_{5000} was shorter than that of PEG_{5000}-*b*-PLA_{5000}, which demonstrated the conjugation of targeting moiety OCT to the PEG-*b*-PLA copolymer. The polydispersity values of the two peaks were less than 1.5, indicating a narrow distribution of molecular weights of the copolymers.

The CMC value of PEG_{5000}-*b*-PLA_{5000} and OCT-PEG_{6000}-*b*-PLA_{5000} was 0.914×10^{-7} mol/L and 4.072×10^{-7} mol/L, respectively. These values are rather low, which is favorable for the formation of micelles.

Characterization of OCT-PM-DTX, PM-DTX, OCT-PM-DiI and PM-DiI

The mean particle size of OCT-PM-DTX and PM-DTX was 69–76 nm (PDI≤0.200), and the DTX encapsulation efficiency was 87% and 98%, respectively (Table I). The final concentration of DTX encapsulated in micelles was around 0.45 mg/ml. The DTX-loaded micelles were stable at 4°C for more than two weeks with little changes in particle size and drug loading amount. The particle size of OCT-PM-DiI and PM-DiI was 51–61 nm (PDI≤0.07), and the DiI encapsulation efficiency was 87% and 94%, respectively (Table I). As also listed in Table I, the Zeta potential of blank PEG_{5000}-*b*-PLA_{5000} micelles was close to zero, while the micelles loaded with DTX or DiI were negatively charged, but their Zeta potential were less than −3 mV.

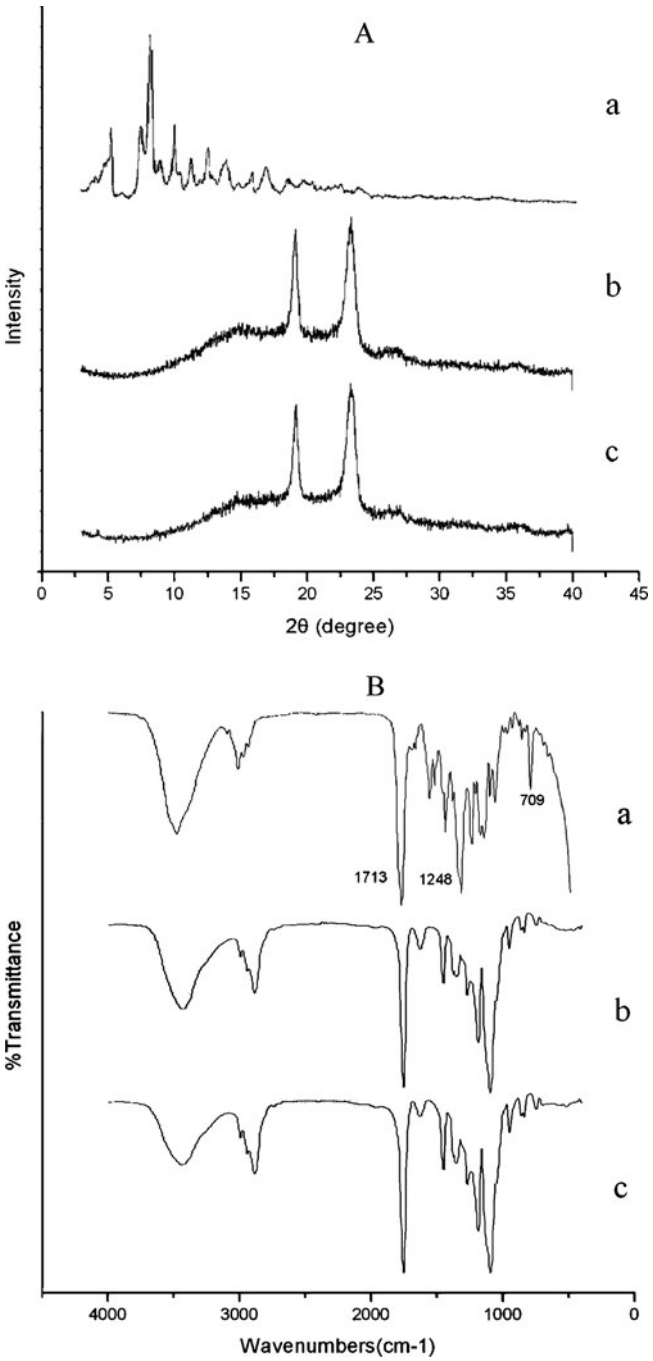

Fig. 4 XRD and FTIR curves of drug-loaded micelles. (**A**) XRD curves of (*a*) DTX, (*b*) lyophilized blank PEG-*b*-PLA micelles, (*c*) lyophilized PM-DTX; (**B**) FTIR curves of (*a*) DTX, (*b*) lyophilized blank PEG-*b*-PLA micelles, (*c*) lyophilized PM-DTX.

All experiments were repeated three times for each group, and the data were expressed as mean ± SD. The accuracy and precision of the measurements are within 2%.

The TEM micrographs showed that the micelle particles were spherical in shape and homogenously dispersed in aqueous solution without aggregation (Fig. 3). The particle size of OCT-PM-DTX was slightly larger than that of PM-DTX, which was in good accord with previous observation by DLS (Table I). In short, a stable micellar system with small particle size, homogenous dispersion, low surface potential and high encapsulation efficiency was obtained.

X-ray diffraction curves and the FTIR spectra a illustrated in Fig. 4. The blank micelles were amorphous, so they showed a relatively wide and broad peak in X-ray diffraction curves (Fig. 4Ab), while the DTX crystals exhibited many distinct sharp peaks (Fig. 4Aa), which disappeared in the DTX-loaded micelles (Fig. 4Ac), indicating that DTX exists in the inner core of micelles in a molecular or amorphous dispersion with little leakage.

As presented in Fig. 4B, DTX showed the characteristic bands at 1713, 1248 and 709 cm^{-1}, as well as the benzene ring bands at 1450, 1500 and 1600 cm^{-1}. After DTX encapsulated in micelles, besides the peak position similar to DTX and blank PEG-*b*-PLA micelles, no new peaks occurred in PM-DTX, and the positions of DTX peaks did not changed obviously in 4Bc, revealing that DTX was

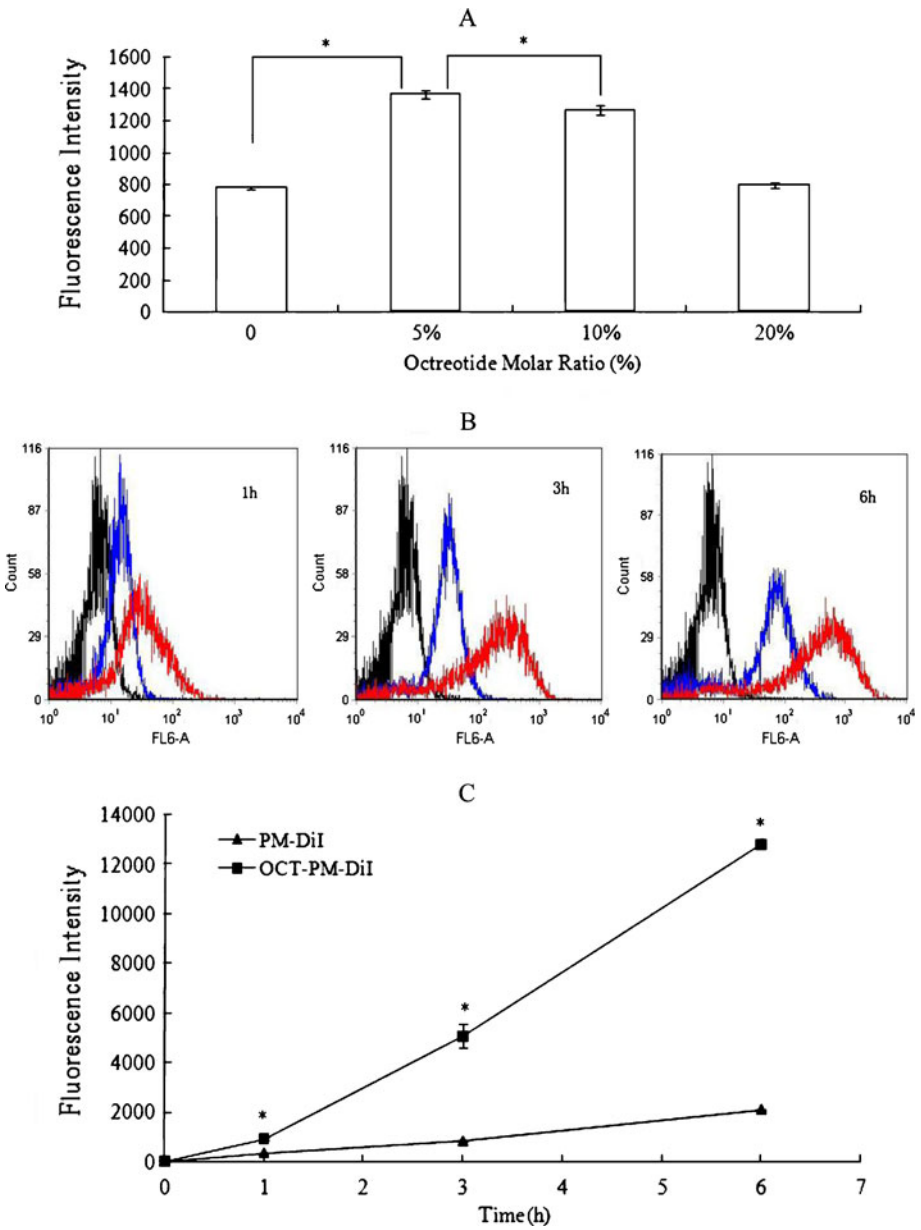

Fig. 5 Flow cytometry studies of OCT-PM-DiI and PM-DiI in NCI-H446 tumor cells. (**A**) Intracellular delivery efficiencies of targeted PEG-*b*-PLA micelles modified by different mol ratio of octreotide. * $p < 0.01$ (**B**) Flow cytometry graph after incubating with OCT-PM-DiI and PM-DiI for 1 h, 3 h and 6 h at 37°C. Black represents untreated NCI-H446 cells as negative control, blue represents PM-DiI, and red represents OCT-PM-DiI. (**C**) Intracellular delivery efficiencies of OCT-PM-DiI and PM-DiI after incubating for 1 h, 3 h and 6 h at 37°C. * $p < 0.01$, OCT-PM-DiI *versus* PM-DiI. Each point represents mean ± SD ($n = 3$).

physically entrapped in the polymer matrix, and there was no chemical interaction between DTX and the copolymers in the micelle preparation process.

Flow Cytometry Studies

It was found that the micelles modified with 5% OCT displayed the highest intracellular delivery efficiency among all the micelles modified by different mol ratio of OCT after incubating with NCI-H446 cells for the same time (Fig. 5A). Based on this result, we prepared the OCT-PM-DiI and OCT-PM-DTX with OCT modification of 5% mol ratio for further experiments.

The intracellular fluorescence intensity exhibited a time-dependent course for both Dil formulations. The intracellular Dil fluorescence intensity increased from 1 h to 6 h as shown in Fig. 5B. It is important to mention that OCT-PM-DiI had 1.5-, 5.1-, 5.1-folds higher internalized DiI fluorescence intensity than that of PM-DiI (Fig. 5C) after 1 h, 3 h, 6 h incubation at 37°C, respectively, indicating the promotion of cell uptake by OCT modification on the surface of micelles.

Confocal Microscopy Studies

As shown in Fig. 6A, D, B, and E, OCT-PM-DiI group displayed stronger fluorescence intensity of DiI in cell cytoplasm than that of PM-DiI group, suggesting again that OCT-modified micelles had higher intracellular delivery efficiency than the non-targeted micelles.

Pre-incubation with goat anti-human SSTR2 polyclonal antibody (1:150), to a large extent, inhibited the intracellular delivery of OCT-PM-DiI. In fact, the intracellular uptake efficiency, in such a case, was even lower than that of non-targeted micelles due to the receptor competitive inhibition effect. In conclusion, this test proved that the mechanism that enhanced intracellular delivery of OCT-PM-DiI was owing to the SSTR2-mediated endocytosis.

Pharmacodynamic Studies

It was demonstrated in Fig. 7A that OCT-PM-DTX group exhibited the highest antitumor efficacy compared to other formulations in terms of retardation of tumor growth. The

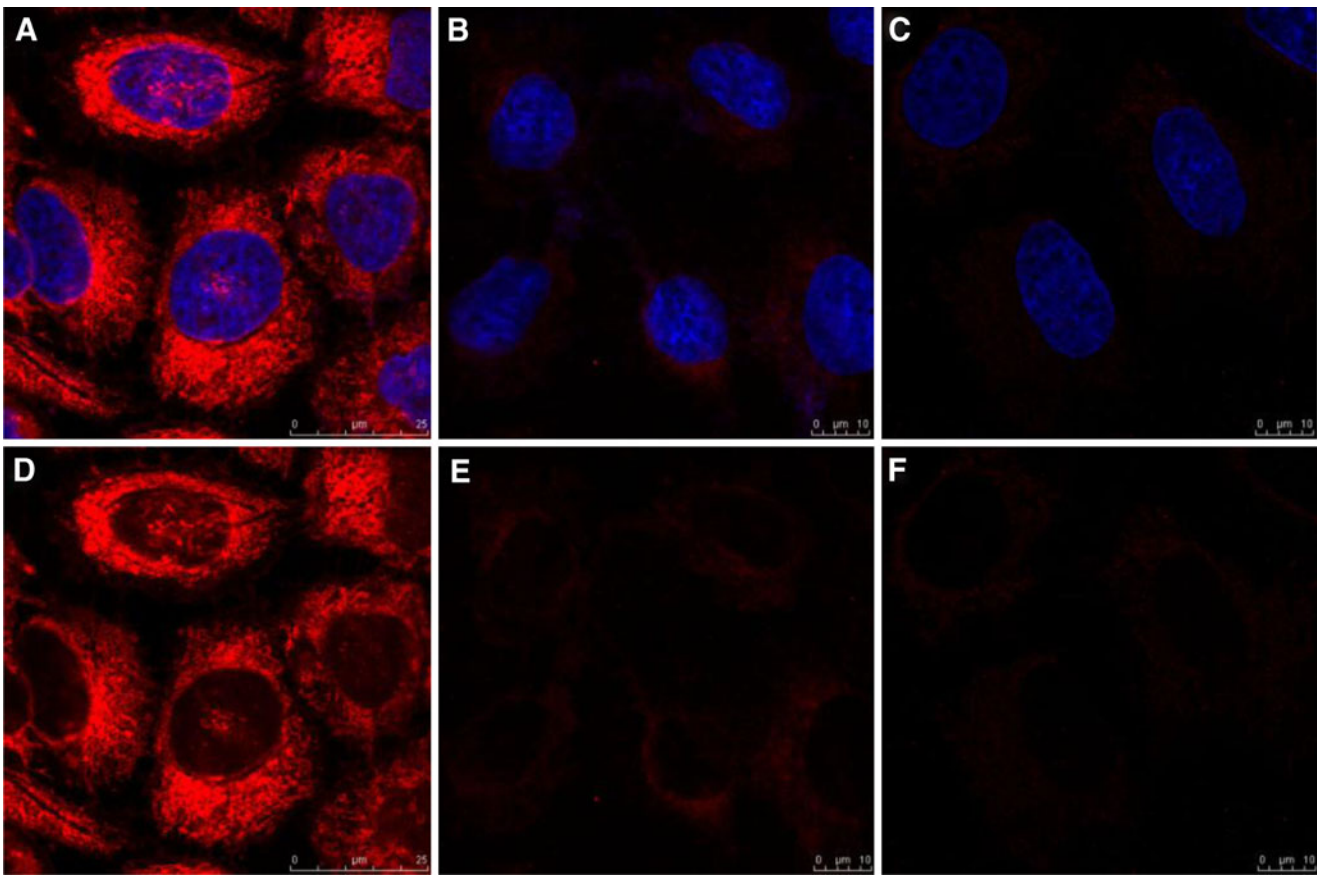

Fig. 6 Confocal microscopy images of NCI-H446 cells incubated with (**A**, **D**) OCT-PM-DiI, (**B**, **E**) PM-DiI and (**C**, **F**) OCT-PM-DiI pre-incubating with goat anti-human SSTR2 polyclonal antibody (1:150) for 3 h at 37°C. Red represents the fluorescence of DiI. Blue represents the fluorescence of Hoechst 33258. **D**, **E**, **F** are the same images as **A**, **B**, **C** without nucleus' overlay.

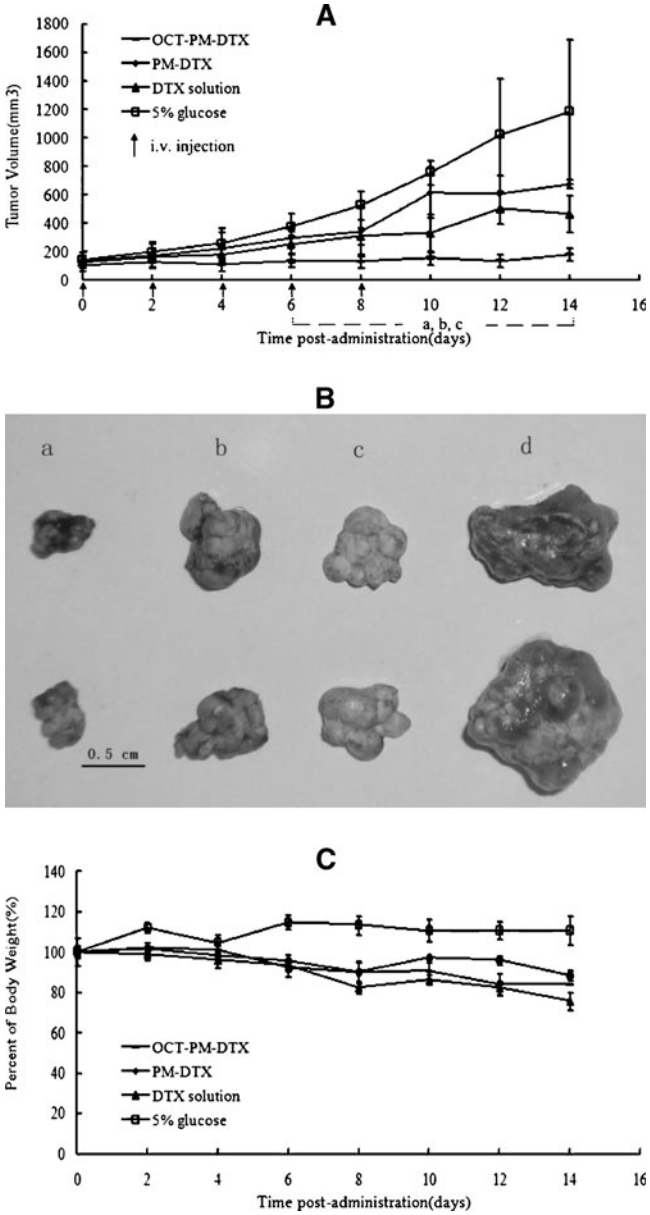

Fig. 7 Pharmacodynamic studies. (**A**) Antitumor activity on NCI-H446 bearing BALB/c male nude mice treated with different formulations. Data represent mean ± SD ($n = 5$). *a* $p < 0.01$, OCT-PM-DTX *versus* 5% glucose at the same time point; *b* $p < 0.01$, OCT-PM-DTX *versus* DTX solution at the same time point; *c* $p < 0.01$, OCT-PM-DTX *versus* PM-DTX at the same time point. (**B**) Photos of stripped solid tumors. *a* OCT-PM-DTX; *b* PM-DTX; *c* DTX solution; *d* 5% glucose as negative control. (**C**) Body weight changes on NCI-H446 xenografts ($n = 5$).

tumor size of OCT-PM-DTX group at the end of the experiment was smaller than other treatment groups (Fig. 7B). Based on the tumor sizes, there seemed to be no difference in tumor growth suppression between the PM-DTX and DTX injection groups. Finally, the three DTX formulations showed similar body weight changes in BALB/c nude mice bearing NCI-H446 tumors (Fig. 7C), revealing that the micelle system and the OCT modification did not increase *in vivo* toxicity.

DISCUSSION

Synthesis and Characterization of OCT-Modified Block Copolymer

As seen in Fig. 2B, GPC test revealed that both PEG_{5000}-*b*-PLA_{5000} and OCT-PEG_{6000}-*b*- PLA_{5000} had narrow distribution peaks, with polydispersity values less than 1.5, indicating that the two copolymers had the uniform distribution of molecular chain length, which could facilitate the formation of uniform micelles. This may be the reason for homogenous dispersion of nanoparticles in size as shown in the TEM micrographs (Fig. 3). It was noticed that both OCT-modified and non-modified block copolymers had low CMC values, less than 10^{-6} mol/L (31), which ensures that the DTX-loaded micelles retain their stable core-shell structure in the bloodstream, even though they would be largely diluted by the blood after intravenous injection. In addition, micelles with low CMC values may achieve longer circulation time *in vivo*, with little drug leakage from the micellar core before the nanoparticles accumulate to the tumor site. On the other hand, limited leakage of DTX from micelle vectors can prevent the released DTX from aggregating and forming crystals in blood circulation, which commonly occurrs in conventional DTX formulations.

Characterization of OCT-PM-DTX, PM-DTX OCT-PM-DiI and PM-DiI

The particle size, Zeta potential and encapsulation efficiency of OCT-PM-DiI and PM-DiI were generally similar to those of OCT-PM-DTX and PM-DTX (Table I), which is important because particle size, surface potential and other physicochemical properties of micelles were proven to be responsible for their behavior *in vitro* and *in vivo* (32). The slight difference between DiI and DTX-loaded micelles indicated that the fluorescent DiI-labeled micelles could be used to study the intracellular delivery behaviors *in vitro*, instead of DTX-loaded PEG-*b*-PLA polymeric micelles.

Flow Cytometry Studies

It was found that the targeted micelles showed higher intracellular uptake than that of non-targeted micelles, although the two kinds of DiI-loaded micelles were very similar in physicochemical properties as listed in Table I (Fig. 5B, C). The effect of their physicochemical properties on the intracellular DiI delivery seems not significant in the test condition.

As we can seen in Fig. 5C, the intracellular fluorescence intensity of DiI in OCT-PM-DiI group was about 5-folds

higher than that of PM-DiI at 3 h and 6 h. In other words, more than 80% of intracellular Dil was due to the receptor-mediated cell uptake of micelles. Hence, it seems reasonable to conclude that OCT modification on the surface of micelles is the main cause for the difference between targeted and non-targeted vectors in terms of their interaction with cells over-expressing SSTRs.

Additionally, the micelles modified with 5% of OCT showed the highest intracellular delivery (Fig. 5A). Namely, relatively lower ligand density appeared to be more effective. A likely explanation may be the steric hindrance at the binding sites between the receptor and ligand (33). A similar finding has been reported previously for the lactose-conjugated polymer micelles (34).

Confocal Microscopy Studies

It was revealed in Fig. 6 that OCT-PM-DiI group displayed stronger internalized DiI fluorescence than that of PM-DiI group. That is to say, the qualitative data in confocal microscopy studies was consistent well with the quantitative one in flow cytometry test (Fig. 5) discussed above.

In addition, in the receptor competitive inhibition experiment, when the tumor cells were pre-incubated with the goat anti-human SSTR2 polyclonal antibody for 1 h before incubation with OCT-PM-DiI, the intracellular DiI fluorescence intensity decreased dramatically, as demonstrated in Fig. 6C and F. This was because the primary antibody previously occupied the somatostatin receptor locus on NCI-H446 cell membrane, leading to the loss of opportunity for OCT to interact with the receptor molecules.

Interestingly, it was observed in the same test (Fig. 6C and F) that receptor competitive inhibition resulted in even lower intracellular DiI fluorescence in OCT-PM-DiI group than that in PM-DiI group. Although the reason is not clear, the steric obstacles from OCT on the micelles and primary antibody associated on the cells are speculated.

Pharmacodynamic Studies

With Tween 80 in the formulation, the DTX injection is a micelle system of surfactants. The PM-DTX and DTX injection exhibited similar anticancer effect (Fig. 7), possibly because both were non-targeted micelle vectors.

It is worthwhile to mention that the dosage of DTX in this study was all reduced to 2.5 mg/kg, one quarter of the normal dosage (10 mg/kg) for the DTX nanoparticles reported (35). Notwithstanding, all formulations showed obvious antitumor effect. The reduction of the DTX dosage could be favorable for decreasing the toxicity to normal tissues.

Above all, OCT-PM-DTX demonstrated better antitumor efficacy than all other groups. Based on the previous studies in cell level, it would be supposed that such system targets DTX to tumor tissue and delivers drug into tumor cells through a somatostatin receptors-mediated endocytosis, resulting in improved anticancer effect.

CONCLUSION

In this study, OCT-modified PEG-*b*-PLA micelles demonstrated higher intracellular drug delivery over non-targeted micelles on SSTRs overexpressing NCI-H446 tumor cells via the somatostatin receptors-mediated endocytosis. Furthermore, the OCT-PM-DTX achieved greater antitumor efficacy *in vivo* than that of non-targeted one, due to the facilitation of the receptors specific intracellular transport of DTX into target tumor cells. It is concluded that the octreotide may be used as a cancer cells recognition moiety for tumor targeting, OCT-modified PEG-*b*-PLA micelles may serve as a promising nanocarrier for hydrophobic anticancer drugs, and OCT-modified micelles loaded with DTX are a potential drug delivery system for malignant solid tumors.

ACKNOWLEDGMENTS

This study was supported by projects from Ministry of Science and Technology, PR China (No. 2009CB930300, No. 2007AA021811, No. 2009ZX09310-001). We thank Dr. Jinfeng Du for his help in preparing the graphs of the manuscript.

REFERENCES

1. Engels FK, Mathot RA, Verweij J. Alternative drug formulations of docetaxel: a review. Anticancer Drugs. 2007;18:95–103.
2. Baker J, Ajani J, Scotte F, Winther D, Martin M, Aapro MS, *et al.* Docetaxel-related side effects and their management. Eur J Oncol Nurs. 2009;13:49–59.
3. Liu B, Yang M, Li R, Ding Y, Qian X, Yu L, *et al.* The antitumor effect of novel docetaxel-loaded thermosensitive micelles. Eur J Pharm Biopharm. 2008;69:527–34.
4. Han X, Liu J, Liu M, Xie C, Zhan C, Gu B, *et al.* 9-NC-loaded folate-conjugated polymer micelles as tumor targeted drug delivery system: preparation and evaluation *in vitro*. Int J Pharm. 2009;372:125–31.
5. Shao K, Huang R, Li J, Han L, Ye L, J. Lou, *et al.* Angiopep-2 modified PE-PEG based polymeric micelles for amphotericin B delivery targeted to the brain. J Control Release. 2010; 147: 118-26.
6. Xiong XB, Uludag H. A. Lavasanifar. Virus-mimetic polymeric micelles for targeted siRNA delivery. Biomaterials. 2010; 31: 5886-93.
7. Torchilin VP. Targeted polymeric micelles for delivery of poorly soluble drugs. Cell Mol Life Sci. 2004;61:2549–59.
8. Kwon GS. Polymeric micelles for delivery of poorly water-soluble compounds. Crit Rev Ther Drug Carrier Syst. 2003;20:357–403.

9. Lin WJ, Chen YC, Lin CC, Chen CF, Chen JW. Characterization of pegylated copolymeric micelles and *in vivo* pharmacokinetics and biodistribution studies. J Biomed Mater Res B Appl Biomater. 2006;77:188–94.
10. Maeda H. The enhanced permeability and retention (EPR) effect in tumor vasculature: the key role of tumor-selective macromolecular drug targeting. Adv Enzyme Regul. 2001;41:189–207.
11. Ishihara T, Kubota T, Choi T, Takahashi M, Ayano E, Kanazawa H, *et al.* Polymeric nanoparticles encapsulating betamethasone phosphate with different release profiles and stealthiness. Int J Pharm. 2009;375:148–54.
12. Liu J, Zeng F, Allen C. Influence of serum protein on polycarbonate-based copolymer micelles as a delivery system for a hydrophobic anti-cancer agent. J Control Release. 2005;103:481–97.
13. Patel YC. Somatostatin and its receptor family. Front Neuroendocrinol. 1999;20:157–98.
14. Virgolini I, Traub T, Novotny C, Leimer M, Fuger B, Li SR, *et al.* Experience with indium-111 and yttrium-90-labeled somatostatin analogs. Curr Pharm Des. 2002;8:1781–807.
15. Weinerand RE, Thakur ML. Radiolabeled peptides in oncology: role in diagnosis and treatment. BioDrugs. 2005;19:145–63.
16. Appetecchiaand M, Baldelli R. Somatostatin analogues in the treatment of gastroenteropancreatic neuroendocrine tumours, current aspects and new perspectives. J Exp Clin Cancer Res. 29:19.
17. Kaltsas GA, Papadogias D, Makras P, Grossman AB. Treatment of advanced neuroendocrine tumours with radiolabelled somatostatin analogues. Endocr Relat Cancer. 2005;12:683–99.
18. Sharmaand K, Srikant CB. Induction of wild-type p53, Bax, and acidic endonuclease during somatostatin-signaled apoptosis in MCF-7 human breast cancer cells. Int J Cancer. 1998;76:259–66.
19. Reynaert H, Rombouts K, Vandermonde A, Urbain D, Kumar U, Bioulac-Sage P, *et al.* Expression of somatostatin receptors in normal and cirrhotic human liver and in hepatocellular carcinoma. Gut. 2004;53:1180–9.
20. Reubi JC. Peptide receptors as molecular targets for cancer diagnosis and therapy. Endocr Rev. 2003;24:389–427.
21. Huang CM, Wu YT, Chen ST. Targeting delivery of paclitaxel into tumor cells via somatostatin receptor endocytosis. Chem Biol. 2000;7:453–61.
22. Watt HL, Kharmate G, Kumar U. Biology of somatostatin in breast cancer. Mol Cell Endocrinol. 2008;286:251–61.
23. Dasgupta P. Somatostatin analogues: multiple roles in cellular proliferation, neoplasia, and angiogenesis. Pharmacol Ther. 2004;102:61–85.
24. Xiong XB, Huang Y, Lu WL, Zhang X, Zhang H, Nagai T, *et al.* Enhanced intracellular delivery and improved antitumor efficacy of doxorubicin by sterically stabilized liposomes modified with a synthetic RGD mimetic. J Control Release. 2005;107:262–75.
25. Erchegyi J, Kastin AJ, Zadina JE. Isolation of a novel tetrapeptide with opiate and antiopiate activity from human brain cortex: Tyr-Pro-Trp-Gly-NH2 (Tyr-W-MIF-1). Peptides. 1992;13:623–31.
26. Beghein N, Rouxhet L, Dinguizli M, Brewster ME, Arien A, Preat V, *et al.* Characterization of self-assembling copolymers in aqueous solutions using Electron Paramagnetic Resonance and Fluorescence spectroscopy. J Control Release. 2007;117:196–203.
27. Elsabahy M, Perron ME, Bertrand N, Yu GE, Leroux JC. Solubilization of docetaxel in poly(ethylene oxide)-block-poly(butylene/styrene oxide) micelles. Biomacromolecules. 2007;8:2250–7.
28. Yang M, Ding Y, Zhang L, Qian X, Jiang X, Liu B. Novel thermosensitive polymeric micelles for docetaxel delivery. J Biomed Mater Res A. 2007;81:847–57.
29. Xiong XB, Mahmud A, Uludag H, Lavasanifar A. Conjugation of arginine-glycine-aspartic acid peptides to poly(ethylene oxide)-b-poly(epsilon-caprolactone) micelles for enhanced intracellular drug delivery to metastatic tumor cells. Biomacromolecules. 2007;8:874–84.
30. Zeng F, Lee H, Allen C. Epidermal growth factor-conjugated poly (ethylene glycol)-block- poly(delta-valerolactone) copolymer micelles for targeted delivery of chemotherapeutics. Bioconjug Chem. 2006;17:399–409.
31. Sezgin Z, Yuksel N, Baykara T. Preparation and characterization of polymeric micelles for solubilization of poorly soluble anticancer drugs. Eur J Pharm Biopharm. 2006;64:261–8.
32. Gu JC, Qiao MX, Gao W, Zhao XL, Hu HY, Xu J, *et al.* Preparation of adriamycin-loaded temperature/pH sensitive self-assembly block copolymer micelles. Yao Xue Xue Bao. 2009;44:793–7.
33. Cairo CW, Gestwicki JE, Kanai M, Kiessling LL. Control of multivalent interactions by binding epitope density. J Am Chem Soc. 2002;124:1615–9.
34. Jule E, Nagasaki Y, Kataoka K. Lactose-installed poly(ethylene glycol)-poly(d, l-lactide) block copolymer micelles exhibit fast-rate binding and high affinity toward a protein bed simulating a cell surface. A surface plasmon resonance study. Bioconjug Chem. 2003;14:177–86.
35. Hwang HY, Kim IS, Kwon IC, Kim YH. Tumor targetability and antitumor effect of docetaxel-loaded hydrophobically modified glycol chitosan nanoparticles. J Control Release. 2008; 128: 23-31.
36. Taxotere® Prescribing Information. Bridgewater, NJ: sanofi-aventis U.S. LLC; Rev. December 2006.